

SYSTEMATIC CONTINUUM ERRORS IN THE LYMAN-ALPHA FOREST AND THE MEASURED TEMPERATURE-DENSITY RELATION

KHEE-GAN LEE

Department of Astrophysical Sciences, Princeton University, Princeton, New Jersey 08544, USA

Second revised draft; Submitted to ApJ

ABSTRACT

Continuum fitting uncertainties are a major source of error in estimates of the temperature-density relation (usually parametrized as a power-law, $T \propto \Delta^{\gamma-1}$) of the inter-galactic medium (IGM) through the flux probability distribution function (PDF) of the Lyman- α forest. Using a simple order-of-magnitude calculation, we show that few percent-level systematic errors in the placement of the quasar continuum due to e.g. a uniform low-absorption Gunn-Peterson component, could lead to errors in γ of order unity. This is quantified further using a simple semi-analytic model of the Ly α forest flux PDF. We find that under-(over-)estimates in the continuum level can lead to a lower (higher) measured value of γ . By fitting models to mock data realizations generated with current observational errors, we find that continuum errors can cause a systematic bias in the estimated temperature-density relation of $\langle \delta(\gamma) \rangle \approx -0.1$, while the error is increased to $\sigma_\gamma \approx 0.2$ compared to $\sigma_\gamma \approx 0.1$ in the absence of continuum errors.

Subject headings: intergalactic medium — quasars: absorption lines — methods: data analysis

1. INTRODUCTION

Over the past two decades, the Lyman- α (Ly α) forest in the line-of-sight to distant quasars has emerged as one of the most important probes of the high-redshift ($z > 2$) universe (see, e.g., Croft et al. 1998; McDonald et al. 2000; Croft et al. 2002; Zaldarriaga et al. 2003; McDonald et al. 2005). This has been underpinned by theoretical advances that established the Ly α forest as arising from neutral hydrogen embedded in a warm photo-ionized intergalactic medium (IGM), tracing the density fluctuations due to gravitational instability in hierarchical clustering cosmological models (see, e.g., Cen et al. 1994; Miralda-Escudé et al. 1996; Davé et al. 1999; Theuns et al. 1998).

In recent years, the Ly α forest is increasingly being used to gain a more detailed understanding of the intergalactic medium. In particular, the thermal history of the IGM holds the key to understanding hydrogen and He II reionization at $z > 6$ and $z \sim 3$, respectively. For an underlying density distribution, $\Delta(x) = \rho(x)/\bar{\rho}$, the astrophysics of the IGM mediates the optical depth of the Ly α forest.

In the standard photoionization equilibrium model of the Ly α forest (Gunn & Peterson 1965), the thermal properties of the IGM are usually described in terms of 3 main parameters: the ionization rate of the photoionizing background radiation, Γ , the temperature of the gas at mean density, T_0 , and the temperature-density relationship¹ approximated as a power-law, $T = T_0 \Delta^{\gamma-1}$.

Various authors have placed constraints on the background ionization rate, Γ , of the IGM using the effective optical depth, τ_{eff} , of the Ly α forest (Bolton et al. 2005; Faucher-Giguère et al. 2008a) and the quasar prox-

imity effect (Scott et al. 2000; Dall’Aglia et al. 2009). Constraints on T_0 have been made using detailed line-profile fitting of individual Ly α absorption lines from high-resolution spectra (see, e.g., Schaye et al. 2000; Becker et al. 2011).

Meanwhile, the probability distribution function (PDF) of the transmitted Ly α forest flux (Jenkins & Ostriker 1991) has been used to place constraints on the temperature-density relation of the IGM. Using this technique, Becker et al. (2007), Bolton et al. (2008), and Viel et al. (2009) have recently found evidence of a highly inverted temperature-density relation, $\gamma \sim 0.5$, in the Ly α forest at $z \sim 2-3$. While some theories (e.g., Furlanetto & Oh 2008) predict a mildly-inverted temperature-density relation ($\gamma \approx 0.8$) as a consequence of inside-out He II reionization, the amount of energy that needs to be injected into the IGM to obtain $\gamma \sim 0.5$ is inconsistent with the observational constraints on heating sources that those redshifts (McQuinn et al. 2009).

Although various systematics such as continuum fitting errors, noise and metal line contamination can bias the interpretation of the flux PDF, high-resolution ($R \equiv \lambda/\Delta\lambda \sim 10^4$) and high signal-to-noise ($S/N \gtrsim 50$ per pixel) Ly α forest spectra can ameliorate these effects (see, e.g., Kim et al. 2007). With such data, metal lines in the Ly α forest region can be directly identified and removed, while the low pixel noise allows precise determinations of the continuum from the peaks of the observed Ly α transmission, with random errors as low as 1–2%.

However, depending on the underlying properties of the IGM, a uniform Gunn-Peterson absorption component² could exist in the Ly α forest even at relatively

² While this term may be reminiscent of the obsolete picture of the IGM as a two-phase medium consisting of dense and cool Ly α clouds embedded in a hot, tenuous inter-cloud medium (Sargent et al. 1980), in this paper we merely use this term to refer generically to a uniform or large-scale low-absorption component in the Ly α forest transmission field.

lee@astro.princeton.edu

¹ The temperature-density relationship of the IGM is often called the ‘equation of state’. This is technically incorrect as the equation of state of the IGM is that of a perfect gas, thus in this Letter we do not use this term.

low redshifts ($z \sim 3$). In such a case, a continuum fitted to the transmission peaks of the observed Ly α forest flux could underestimate the continuum, since few of the peaks would reach the true quasar continuum. This *systematic* continuum bias could exist even in high-S/N spectra which have small *random* errors in the pixel fluxes. Workers in this field are aware of this possibility: Bolton et al. (2008) tested this by fitting their flux PDFs with the continuum raised by 1.5% and 5%, but found that these provided worse fits to their data. Becker et al. (2007) and Viel et al. (2009) made the continuum level a free parameter in their likelihood analysis, although neither found a significant continuum bias.

However, none of the aforementioned studies tried to directly estimate the amount of continuum bias at low-redshift ($z \lesssim 3-4$), nor is it well-understood how such a bias could affect measurements of the IGM temperature-density relation.

In a paper measuring the effective optical depth τ_{eff} of the Ly α forest, Faucher-Giguère et al. (2008b) did attempt to constrain the amount of bias in their continuum fits by hand-fitting mock spectra derived from numerical simulations. They found that even at $z = 3$, continua fitted to the peaks of the transmission underestimate the level of the continuum by 5%, although they assumed an extreme value of $\gamma = 1.6$ in their mock spectra. While this was the temperature-density relation calculated for a relaxed IGM following hydrogen reionization (Hui & Gnedin 1997), it is not expected to be valid during the epoch of He II reionization at $z \lesssim 3$ (Furlanetto & Oh 2008; McQuinn et al. 2009). Since $\tau_{\text{eff}} = -\ln(\langle F \rangle)$, a systematic bias in the estimated continuum level leads to errors in τ_{eff} at approximately the same level (for example, a 2% underestimate in the continuum would lead to roughly a 2% overestimate in τ_{eff}). In contrast, such continuum errors would bias the estimated temperature-density relation in a more complicated manner, which is not well-understood. This short paper is intended to investigate this bias in a simple, easily-reproducible, manner.

In Section 2 we first make a simple back-of-the-envelope calculation which indicates that systematic biases in the continuum fitting of even a few percent could cause large errors in the estimated temperature-density relation. Section 3 then introduces a simple semi-analytic model of the Ly α forest flux PDF to quantify this error, followed by a discussion (Section 4) of these biases and some methods to correct for them.

2. SIMPLE ESTIMATES

In this section we make an order-of-magnitude calculation of the bias in the IGM temperature-density relation that could potentially arise from systematic errors in the placement of the quasar continuum level. We first define the fractional continuum error,

$$f_c = \frac{C_{\text{est}} - C_{\text{true}}}{C_{\text{true}}}, \quad (1)$$

where C_{true} is the true quasar continuum in the Ly α forest, while C_{est} is the estimated continuum.

The flux transmission through the IGM F is related to the intervening optical depth τ by $F = \exp(-\tau)$, while τ is in turn related to the underlying matter distribution, $\Delta(x) \equiv \rho(x)/\bar{\rho}$.

For this calculation we use the fluctuating Gunn-Peterson approximation (FGPA, see, e.g., Croft et al. 1998),

$$\tau = \tau_0 \Delta^{2-\alpha}, \quad (2)$$

where $\Delta \equiv \Delta(x)$, $\alpha = 0.7(\gamma - 1)$, and τ_0 is a factor which includes astrophysics such as the Ly α recombination coefficient and the photoionizing UV background Γ . Here we assume τ_0 to be constant, so that the only unknown parameter of the IGM is the exponent α in the equation of state.

We rearrange Equation 2 to

$$\alpha = \frac{\ln \tau_0 - \ln \tau}{\ln \Delta} + 2. \quad (3)$$

The derivative of α with respect to τ is then

$$\frac{d\alpha}{d\tau} = -\frac{1}{\tau \ln \Delta}. \quad (4)$$

This allows us to estimate the error in the derived equation of state, $\delta\alpha \equiv \alpha^{\text{est}} - \alpha^{\text{true}}$ (the superscripts ‘est’ and ‘true’ refer to the estimated and true underlying quantities respectively), arising from a systematic error in the measured optical depth $\delta\tau$ for a given matter overdensity Δ :

$$\begin{aligned} \delta\alpha &\sim -\frac{1}{\ln \Delta} \frac{\delta\tau}{\tau} \\ &\sim \frac{\delta\tau}{\tau}. \end{aligned} \quad (5)$$

In the second line, we have approximated $-\ln \Delta$ to be of order unity, since the low-absorption regions of the IGM are in the underdense ($\Delta < 1$) parts of the universe.

Now consider the effects of a misestimated quasar continuum level C_{est} , where C_{true} is the true continuum level. Faucher-Giguère et al. (2008b) have shown that the true optical depth τ^{true} is related to the measured optical depth corresponding to the underestimated continuum, τ^{est} by

$$\begin{aligned} \delta\tau &= \tau^{\text{est}} - \tau^{\text{true}} \\ &= \ln \left(1 + \frac{C_{\text{est}} - C_{\text{true}}}{C_{\text{true}}} \right) \\ &\simeq f_c, \end{aligned} \quad (6)$$

where in the last line we have substituted in Equation 1 and assumed that it is small ($|f_c| \lesssim 0.1$).

Inserting Equation 6 into Equation 5, and using the fact that in the low-absorption regions $F = \exp(-\tau) \simeq 1 - \tau$, we get

$$\delta\alpha \sim \frac{f_c}{1 - F}. \quad (7)$$

As the strongest constraints on the temperature-density relation of the IGM come from the low-absorption/high-transmission ($1 - F \sim \%$) pixels of the Ly α forest, systematic errors in the continuum estimate of just a few percent can cause large ($\delta\gamma \sim \delta\alpha \sim 1$) errors in the estimated value of γ .

3. MOCK ANALYSIS

In this section, we generate theoretical flux PDFs of the Ly α forest using a simple semi-analytic model, and quantitatively study the errors introduced into the estimated

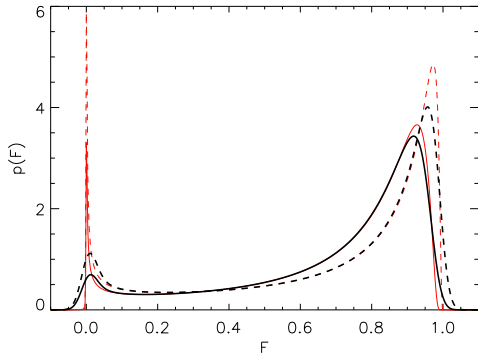


FIG. 1.— Unbinned flux PDFs generated from Eq. 9, with $\gamma = 0.5$ (thin red dashed line) and $\gamma = 1.6$ (thin red solid line). The flux PDFs are normalized to $\langle F \rangle = 0.70$. The thick black lines denote the PDFs after being smoothed by a Gaussian kernel corresponding to $S/N = 50$ in our simplified noise model.

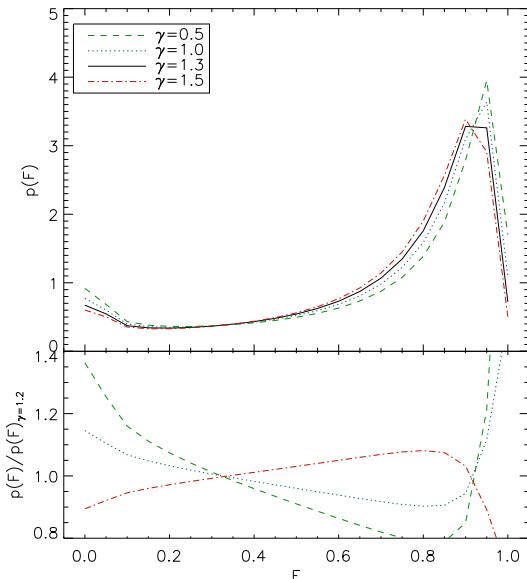


FIG. 2.— (Upper panel) Binned flux PDFs generated from Eq. 9 with different temperature-density relations, $\gamma = 0.5$ (green dashed line), $\gamma = 1.0$ (blue dotted line), $\gamma = 1.2$ (black solid line), and $\gamma = 1.6$ (red dot-dashed line). The lower panel shows the ratio of the various flux PDFs with respect to the $\gamma = 1.0$ model. The relative differences are similar to those presented in Bolton et al. (2008).

temperature-density relation caused by systematic errors in the Ly α forest continuum.

3.1. Toy Flux PDFs

We first generate theoretical flux PDFs by using as a starting point the semi-analytic density PDF from Miralda-Escudé et al. (2000) (hereafter MHR00):

$$p(\Delta)d\Delta = A \exp \left[\frac{-\left(\Delta^{-2/3} - C_0\right)^2}{2(2\delta_0/3)^2} \right] \Delta^{-\beta} d\Delta, \quad (8)$$

where Δ is the matter density, while A , β , C_0 , and δ_0 are redshift-dependent parameters interpolated from the values published in MHR00. At $z = 3$, the corresponding values are $A = 0.558$, $\beta = 2.35$, $C_0 = 0.599$, and $\delta_0 = 1.90$.

The corresponding Ly α forest flux PDF is then derived by substituting in $\Delta(\tau)$ using the FGPA (Equation 2) and then the relation $F = \exp(-\tau)$:

$$p(F)dF = \frac{dF}{F} \frac{A}{\tau_0(2-\alpha)} \left(\frac{-\ln F}{\tau_0} \right)^{\frac{\alpha-1-\beta}{2-\alpha}} \times \exp \left\{ \frac{-\left[\left(-\ln F/\tau_0 \right)^{-\frac{2}{3(2-\alpha)}} - C_0 \right]^2}{2(2\delta_0/3)^2} \right\}. \quad (9)$$

This is then normalized such that $\int_0^1 p(F)dF = 1$.

The parameters in Equation 9 that characterize the IGM are α and τ_0 . τ_0 is a function that depends on the background photoionization rate in the IGM and the temperature at mean density, but for the purposes of this paper we adjust it to yield a fixed value of mean optical depth $\langle F \rangle(z) = \exp(-\tau_{\text{eff}}(z))$ for a given redshift. Thus, at fixed redshift the only free parameter in this model is $\gamma = 1 + \alpha/0.7$ which parametrizes the temperature density equation-of-state.

Note that this model does not correctly account for thermal broadening of the Ly α forest lines, nor peculiar velocities. However, Bolton et al. (2008) have shown from hydrodynamical simulations that the flux PDF is not sensitive to T_0 , which affects the Ly α forest primarily through thermal broadening and by changing the Jean's smoothing scale. Peculiar velocities need to be included to obtain the correct flux PDF shape, but they arise primarily from gravitational collapse of large-scale structure. Thus, we do not expect the omission of peculiar velocities to seriously affect the relative behavior of the flux PDF with changes to the temperature-density relation.

We show the flux PDFs calculated for 2 extreme values, $\gamma = 0.5$ and $\gamma = 1.6$ in Figure 1. $\gamma = 0.5$ corresponds to a highly inverted temperature-density relation, which had been detected by (Becker et al. 2007; Bolton et al. 2008). While $\gamma = 1.6$ is a value calculated by Hui & Gnedin (1997) for a post-reionization relaxed IGM, which should be valid in the epoch between the end of hydrogen reionization and prior to He II reionization, $3 \lesssim z \lesssim 6$.

Figure 1 illustrates the effects of changing γ : at fixed temperature at mean density T_0 , lowering γ increases the temperature in the underdense ($\Delta < 1$) regions of the IGM. This decreases the hydrogen recombination rate, therefore reducing the H I optical depth and increasing the transmission in those regions. The differences are apparent in the $F \gtrsim 0.5$ regions of the PDF, where the peak is shifted to higher F . The probability of having pixels with close to 100% transmission decreases as γ goes up; at $\gamma = 1.6$, the probability drops to zero by $F \simeq 0.98$ (in our model) thus leading to Gunn-Peterson absorption at the 2% level. In this case, the lack of transmission peaks reaching the true continuum level is likely to lead to an underestimate of the continuum, potentially biasing the estimate of γ . Note that the moderate-absorption regions of the PDF ($0.2 \lesssim F \lesssim 0.6$) do not vary much with γ . This agrees with Bolton et al. (2008), who found that using only these moderate-absorption pixels significantly weakens constraints on γ .

The effects of finite signal-to-noise are introduced by smoothing the flux PDF from Equation 9 with a Gaus-

sian kernel. We use a constant smoothing length of $\sigma_{sm} = 1/50$ to simulate an average $S/N = 50$ per pixel, a typical value for high-resolution and high- S/N Ly α forest spectra. This is an acceptable simplification, as Table 3 in McDonald et al. (2000) shows that the typical pixel noise in real data is roughly constant across the different flux bins. Note that the presence of noise scatters some pixels to $F \gtrsim 1$, changing the shape of the flux PDFs (black curves in Figure 1).

We then bin the flux PDFs in the fashion of McDonald et al. (2000) and Kim et al. (2007): the ‘noisy’ flux PDF is divided into 21 bins with size $\Delta F = 0.05$ in the range $0 < F < 1$. The ‘noisy’ portions of the flux PDF with $F < 0$ and $F > 1$ are transferred to the $F = 0$ and $F = 1$ bins, respectively.

In Figure 2, we show the binned PDFs for different temperature-density relations. The overall trend of the unbinned PDFs are similar to that in the unbinned case: the high-transmission peak of the PDF shifts to larger F as γ is decreased. In addition, the number of pixels in the $F = 1.0$ bin increases with decreasing γ . The overall shape of the flux PDFs are in broad agreement with other theoretical flux PDFs published in the literature, including McDonald et al. (2000), Bolton et al. (2008), and White et al. (2010). However, note that we are unable to reproduce the exact shapes of the flux PDFs as seen in the Kim et al. (2007) data, nor from hydrodynamical simulations (e.g., Bolton et al. 2008): our PDFs tend to peak at lower values of F for a given value of γ , while the $\gamma = 0.5$ PDF here does not have the same shape in the high-transmission end obtained from the Bolton et al. (2008) hydrodynamical simulations, in which the PDF peaks in the $F = 1.0$ bin. The MHR-FGPA model also appears to underpredict the number of low-transmission pixels ($F \approx 0$) in comparison with the Bolton et al. (2008) simulations.

In the lower panel of Figure 2, we plot the ratio of the flux PDFs with respect to that with $\gamma = 1.2$. These appear similar to the analogous plots shown in the lower panels of Figures 2 and 4 in Bolton et al. (2008). The main differences are that the flux PDFs in the hydrodynamical simulations pivot at $F \approx 0.1$, while those in our model pivot at a higher value of $F \approx 0.3$. Nevertheless, the *relative* behavior of our model PDFs with respect to γ appear similar to those in the Bolton et al. (2008) hydrodynamical simulations. Since the primary effect of systematic continuum errors is to rescale the flux PDF along the abscissa, the fact that our toy model correctly reproduces the relative changes in the PDF with respect to γ means that it can be used to study continuum errors, even if it should not be used to make direct comparisons with data.

3.2. Effect of Continuum Errors

In this section, we study the effect of systematic continuum biases on the value of γ measured from the mock flux PDFs described above, and the corresponding errors on this estimate. This mock analysis is carried out at a fixed redshift of $z = 3$, an epoch at which Gunn-Peterson absorption is usually assumed to be negligible, but could account for as much as 4-5% of the observed flux (Giallongo et al. 1992; Faucher-Giguère et al. 2008b). All mock PDFs are set to a mean flux of $\langle F \rangle(z = 3) = 0.70$ (Meiksin & White 2004), and the

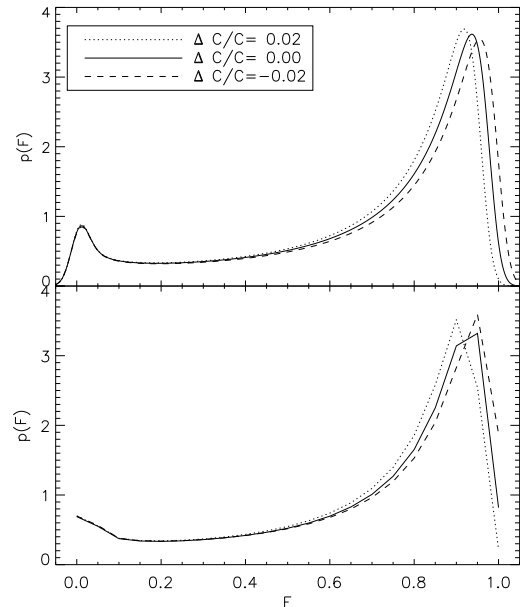


FIG. 3.— The effect of systematic continuum errors on the Ly α forest flux PDF. The top panel shows the unbinned flux PDFs generated with $\gamma = 1.2$ and $S/N = 50$, with no continuum error (black line), 2% overestimated continuum (dotted line), and 2% underestimated continuum (dashed line). The lower panel shows the corresponding flux PDFs in $\Delta F = 0.05$ bins. 2% errors in the continuum determination can drastically change the shape of the binned flux PDF.

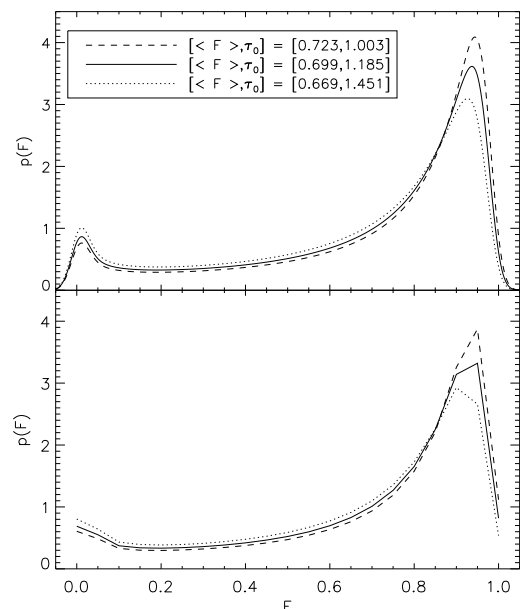


FIG. 4.— The effect of changing τ_0 (or equivalently $\langle F \rangle$) on the flux PDF. The top panel shows the unbinned flux PDFs generated with $\gamma = 1.2$ and $S/N = 50$, with τ_0 adjusted to match the effective mean-flux of the PDFs with the corresponding line-styles in Figure 3. The lower panel shows the corresponding flux PDFs in $\Delta F = 0.05$ bins. τ_0 changes the flux PDF differently from the temperature-density relation or continuum errors. No continuum errors have been applied in these PDFs.

model parameters from Equation 8 are set to $z = 3$.

Systematic continuum errors are introduced into the flux PDFs by multiplying the flux scales with the factor $1 + f_c$ prior to binning — positive values of f_c denote an overestimate with respect to the true continuum, and vice versa. The dotted and dashed curves in Figure 3 illustrate the effects of these errors on a flux PDF with $\gamma = 1.2$. Clearly, just 2% systematic errors in the continuum estimation can dramatically change the shape of the binned flux PDFs: with a 2% underestimate of the continuum, the number of unabsorbed pixels ($F = 1.0$) increases by a factor of two. Note that the continuum errors also change the measured mean-flux $\langle F \rangle$. For the cases with $f_c = [-0.02, 0, 0.02]$, the effective mean-fluxes are $\langle F \rangle = [0.723, 0.699, 0.669]$, respectively. The scatter in these mean-flux values are at the same level as the current observational uncertainty of several percent at $z \approx 3$.

To investigate if the mean-flux might be degenerate with γ and f_c , in Figure 4 we show $\gamma = 1.2$ flux PDFs with τ_0 adjusted to give $\langle F \rangle$ values corresponding to the curves in Figure 3, without continuum errors included. The corresponding values used to generate these PDFs are $\tau_0 = [1.003, 1.185, 1.451]$ for $\langle F \rangle = [0.723, 0.699, 0.669]$, respectively. We see that a smaller τ_0 or higher $\langle F \rangle$ can shift the high-transmission peak of the flux PDF to larger F , analogous to lowering γ . However, the relative ratio of high-absorption/low-transmission pixels ($F < 0.85$), with respect to the low-absorption/high-transmission end ($F > 0.85$) behaves differently with changes in τ_0 compared to when γ or f_c is varied (c.f. Fig. 2 and Fig. 3). This suggests that the degeneracy of τ_0 with respect to γ and f_c can be broken in an analysis of the full flux PDF, but nevertheless τ_0 needs to be taken into account.

To quantify the effects on the estimated temperature-density relation, the flux PDFs with different combinations of $[\gamma, f_c]$ are then compared with mock data PDFs with similar noise properties to the Kim et al. (2007) flux PDFs, which is the best existing data set. However, the bins of the flux PDF are highly correlated, thus one needs a covariance matrix in order to generate random samples with the correct covariances. As our semi-analytic model does not actually result in simulated Ly α forest sightlines, it is problematic to estimate the necessary covariances. Instead, we use the same covariance matrices described in §4.1 of Bolton et al. (2008): the covariance matrix (kindly provided by James Bolton) derived from their $z = 2.94, \gamma = 0.44$ simulations are used to estimate the correlation coefficients between different flux bins. This is then used in conjunction with the errors (i.e. diagonal covariance terms) in the Kim et al. (2007) data to estimate the cross-terms of the final covariance matrix. We then carry out Cholesky decomposition on this covariance matrix to generate random correlated errors, which are then applied to the model flux PDFs. This process assumes that all the model covariances are the same as those in Bolton et al. (2008), but this should be reasonable considering the approximate nature of our analysis.

We can then quantify the effects of continuum bias by sampling the reduced Chi-squared between each mock data PDF, and different model curves with various combinations of γ and f_c . Since the bins are highly corre-

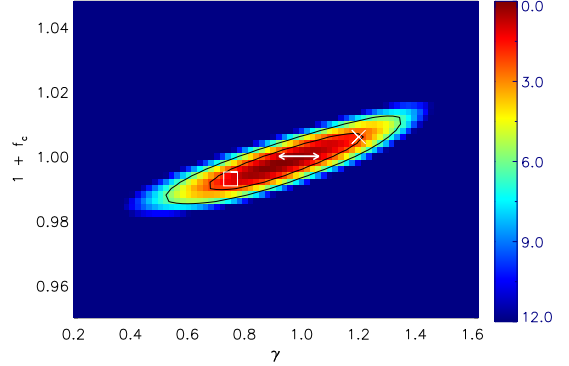


FIG. 5.— Likelihood plots for different combinations of γ and f_c , computed with respect to a mock flux PDFs generated with $\gamma = 1.0$. The contours enclose the 68% and 95% confidence intervals, while the color scale denotes $\Delta\chi^2 \equiv \chi^2 - \chi_{min}^2$. The square and cross denote the extreme values of γ plotted in Figure 6 which constitute acceptable $\sim 1\sigma$ fits to the $\gamma^{true} = 1.0$ mock flux PDF (also plotted in Figure 6) once continuum errors are considered. The white horizontal arrow denotes the 68% confidence interval for γ when the continuum is perfectly known, i.e. $f_c = 0$.

lated, the expression for the Chi-squared is:

$$\chi^2 = [d_i - p_i^{model}]^T C_{ij}^{-1} [d_i - p_i^{model}] \quad (10)$$

where d_i are the bins in the mock data PDFs, p_i^{model} is the model flux PDF with some combination of γ , f_c and τ_0 , while C_{ij} is the covariance matrix discussed above. The confidence level of the various parameter combinations can then be estimated from $\Delta\chi^2 \equiv \chi^2 - \chi_{min}^2$.

In our analysis, we regard the Ly α forest mean-flux, $\langle F \rangle$, (or equivalently within our model, τ_0) as a nuisance parameter to be marginalized over. At each point in the $[\gamma, f_c]$ model parameter space, we marginalize over the mean-flux in the likelihood, $\mathcal{L} \equiv [(2\pi)^N \det C_{ij}]^{-1} \exp\{-(1/2)\chi^2\}$. If we assume the error in the mean-flux is Gaussian, we can then marginalize over the possible mean-flux values $\langle F \rangle'$:

$$\mathcal{L}(\gamma, f_c | \langle F \rangle) \propto \int_{-\infty}^{\infty} \mathcal{L}(\gamma, f_c, \langle F \rangle') \exp\left(-\frac{(\langle F \rangle' - \langle F \rangle)^2}{\sigma_{\langle F \rangle}^2}\right) d\langle F \rangle', \quad (11)$$

where we have used $\langle F \rangle = 0.70$ and $\sigma_{\langle F \rangle} = 0.02$ for $z = 3$. Note that we have ignored normalization factors that will be canceled out when we evaluate $\Delta\chi^2$, and have evaluated the integral using 7-point Gauss-Hermite quadrature.

Figure 5 shows the likelihood plot for fits to a mock data PDF generated with $\gamma^{true} = 1.0$, computed with respect to different combinations of γ and f_c . The contours indicates the 68% and 95% confidence intervals ($\Delta\chi^2 = 2.30$ and $\Delta\chi^2 = 6.17$, respectively). The error ellipse shows a significant degeneracy between γ and f_c . For reference, we also show the 68% confidence level ($\Delta\chi^2 = 1$) in the case where the continuum is not allowed to vary (horizontal white arrows). The range of γ which falls within the 68% confidence interval increases significantly to $\sigma_\gamma = 0.2 - 0.3$ once the continuum level is allowed to vary. Without continuum errors, the error³

³ We use the terms ‘ 1σ errors’ and ‘68% confidence intervals’

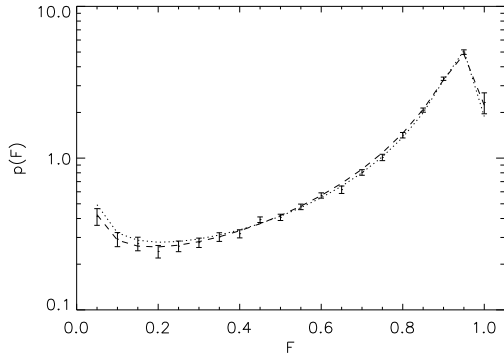


FIG. 6.— Flux PDFs corresponding to Figure 5. The error bars denote the mock $\gamma = 1.0$ flux PDF with simulated scatter, against which the likelihoods in Figure 5 were calculated. The dashed- and dotted lines denote model PDFs with $[\gamma = 0.75, f_c = -0.007]$ and $[\gamma = 1.2, f_c = 0.006]$, which constitute acceptable ($\Delta\chi^2 \approx 2$, 68% confidence level) fits to the mock $\gamma^{\text{true}} = 1.0$ data points. Their respective positions in $[\gamma, f_c]$ space are shown as the square and cross in Fig 5. Note that the ordinate axis is plotted logarithmically in this figure.

in the estimated γ is $\sigma_\gamma \approx 0.05$.

The square and cross symbols in Figure 5 denote two extreme points in the $[\gamma, f_c]$ parameter space that fall within the 68% confidence interval of the underlying flux PDF with $\gamma^{\text{true}} = 1.0$. The binned flux PDFs for these two combinations of $[\gamma, f_c]$ are juxtaposed with the underlying PDF in Figure 6. The similarity of these PDFs with significantly different temperature-density relations ($\gamma = 0.75 - 1.2$) illustrates the effect of continuum errors on the measurement.

Figure 7 shows the average estimated value of γ as a function of the ‘true’ underlying temperature-density power-law γ^{true} and its associated errors, averaged over 40 Gaussian realizations for each value of γ^{true} . The dotted lines denote the average 68% confidence intervals if systematic continuum errors are considered, while the shaded area shows the 1σ intervals if the continuum is known perfectly. We see that continuum errors cause a significant increase in the error on γ : at higher temperature-density slopes ($\gamma \sim 1.5$) the errors increase from $\sigma_\gamma \approx 0.05$ to $\sigma_\gamma^{\text{cont}} \approx 0.15$; at flatter or inverted slopes, the errors are generally larger but still increase from $\sigma_\gamma \approx 0.1$ to $\sigma_\gamma^{\text{cont}} \approx 0.2$. In general, the errors increase by a factor of ~ 2 once we consider continuum errors.

4. DISCUSSION & CONCLUSION

In this paper we have quantified the effect of systematic continuum errors on the temperature-density relation, γ , estimated from the Ly α forest flux PDF, using a simple toy model which correctly reproduces the relative changes in the flux PDF with respect to γ .

We found that small systematic errors of just $\sim 1 - 2\%$ in the overall continuum level can bias the estimated γ to smaller values. In the absence of continuum errors, the 1σ errors on the estimated value of γ is $\sigma_\gamma \approx 0.1$, but with continuum errors this interval is increased to $\sigma_\gamma \approx 0.2$.

interchangeably but the latter is the quantity we have really measured. These two terms would be identical in the case of Gaussian errors.

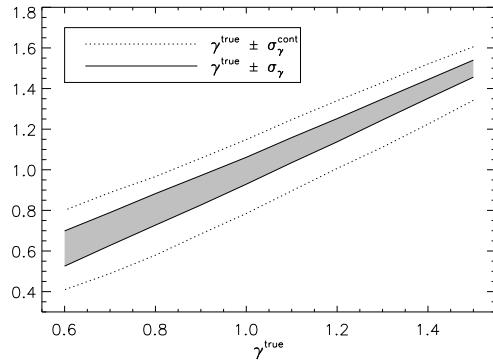


FIG. 7.— The 1σ upper- and lower-limits in the value of γ estimated from mock flux PDFs generated with some underlying value of γ^{true} , when continuum biases are taken into account (dotted lines) and if the continuum is perfectly known (shaded area enclosed by solid lines). Continuum uncertainties roughly double the error on γ . These values are averaged over 40 mock data realizations for each value of γ^{true} .

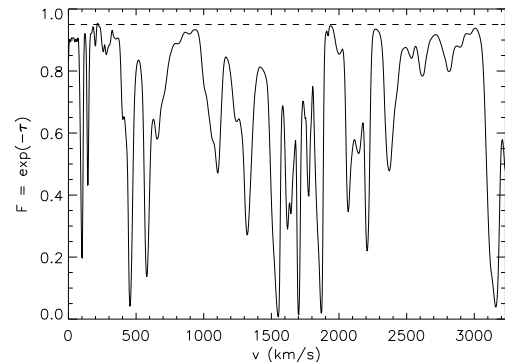


FIG. 8.— A Ly α forest sightline from the Cen & Chisari (2010) hydrodynamical simulations extracted at $z = 3.0$ and smoothed to a resolution of 6.7 km s^{-1} . The dashed horizontal line indicates the $F = 0.95$ flux level. Even though no pixel noise is present, an attempt to fit the continuum to this mock spectrum will likely result in a continuum bias of $f_c \approx -0.05$. Courtesy of R. Cen.

While we have used a simple semi-analytic model to calculate the flux PDFs (although note that this is the same model used by Becker et al. (2007) to analyze their spectra), the relative scaling of the resultant flux PDF with γ is reasonably accurate and thus the biases discussed here are qualitatively valid. We have also marginalized over the mean-flux in our analysis.

In addition, in the simple mock analysis presented here, both the data realizations and ‘theory’ flux PDFs are derived from exactly the same model. In a real data analysis, uncertainties in the underlying physical model (e.g. gas temperature, UV ionizing background, σ_8 , Jeans’ smoothing scale etc.), and other observational uncertainties such as metal contamination must increase the error in γ beyond those presented here.

Another point that should be emphasized is that prior to the biases in γ considered in this paper, systematic continuum errors are not a symmetric effect. Overestimates of the continuum ($f_c > 1$) are less likely with high-quality data — an observer is unlikely to place the continuum level significantly above the observed transmission peaks, whereas low-level Gunn-Peterson absorption can degrade the transmission peaks and lead to

underestimates of the continuum ($f_c < 0$). There is thus an additional bias towards smaller values of γ due to the higher probability of underestimating the continuum rather than overestimating it. In the MHR00 model considered here, the maximum amount of possible Gunn-Peterson absorption is in fact fairly limited at $z = 3$: about 2% with $\gamma = 1.6$ (Figure 1). Other models could provide even more Gunn-Peterson absorption at these redshifts. An example is shown in Figure 8, which plots a $z = 3$ Ly α forest spectrum extracted from the detailed hydrodynamical simulations described in Cen & Chisari (2010). If this were actual data, an observer would probably underestimate the spectrum by 5% even in the absence of noise.

Recent studies of the flux PDF that claimed a highly inverted temperature-density relation (Becker et al. 2007; Bolton et al. 2008; Viel et al. 2009) have considered the possibility of a systematic continuum bias. However, Becker et al. (2007) used the same semi-analytic MHR00 model for the flux PDF used in this paper, which may not accurately capture the details of the Ly α forest flux field at a sufficiently level for data analysis. Bolton et al. (2008) and Viel et al. (2009) both analyzed the same data set from Kim et al. (2007): Bolton et al. (2008) checked for continuum errors by comparing their calculating likelihoods after rescaling their continua by 1.5% and 5%, while Viel et al. (2009) marginalized the continuum in their analysis — both concluded that continuum errors were not significant and that the inverted temperature-density relation was favored. However, it is also interesting to note that Viel et al. (2009) arrived at a best-fit continuum error suggesting an *overestimated* continuum of 1% in the Kim et al. (2007) data (c.f. the random errors in the continuum fitting, $\sigma_{\text{fit}} = 1-2\%$). In other words, they favor a continuum which is *lower* than that which was actually fitted to the Kim et al. (2007) spectra. In the context of our analysis, this would be consistent with an underestimation of γ . We also note that Viel et al. (2009) had fitted for a redshift-independent continuum error when analyzing the Kim et al. (2007) flux PDFs. Since this data set is dominated by lower-redshift ($z < 2.5$) spectra (which should be less affected by low-level Gunn-Peterson absorption), it is possible that the true continuum error cannot be fully accounted for, using a redshift-independent approach.

Considering the controversial nature of the claims of a highly-inverted IGM temperature-density relation, we feel a more direct approach towards dealing with continuum bias is required that had been done previously. There are some possibilities: Giallongo et al. (1992) had

extrapolated a power-law continuum from redwards of the quasar Ly α emission line to estimate the amount of uniform GP absorption in the peaks of the Ly α forest. Existing data sets will allow much stronger constraints to be placed using this method, although it requires the assumption that the mean quasar continuum slope does not change with redshift.

Alternatively, when comparing simulations with data, the simulated sightlines need to be processed through the same continuum-fitting method as the observed data, i.e. through ‘forward-modeling’. Faucher-Giguère et al. (2008b) estimated continuum biases by fitting simulated mock spectra, and comparing these fits with the underlying continuum. However, they were attempting to measure the optical evolution of the Ly α forest, and used simulations with a fixed value of $\gamma = 1.6$. For this method to account for continuum biases in studies exploring a large parameter space, one would need to hand-fit large sets of mock spectra (ideally including realistic quasar continua) covering the explored parameter space. This would be time-consuming, but in principle would be a robust method to account for systematic errors in the continuum fits, especially if automated continuum-fitting methods are used (Dall’Aglia et al. 2009).

Another avenue for improvement to use larger Ly α forest data sets, and hence reduce the errors in the flux PDF and other statistics. The Kim et al. (2007) sample (18 quasars) represent a significant increase in data size in comparison with McDonald et al. (2000) (8 quasars), but considerably more high-resolution, high-S/N spectra than these currently exist. Increasing the sample size would clearly reduce the errors in the measured flux PDF, which would limit the scope of continuum errors to bias the measured temperature-density relation.

At time of writing, the measurement of the inverted temperature-density relation has been carried out by the same group of authors (Bolton et al. 2008; Viel et al. 2009) analyzing the same flux PDF data (Kim et al. 2007). Alternative and independent analyses are urgently required in order to verify this phenomenon, which would have important implications on IGM science as well as energetic sources in the high-redshift universe.

The author thanks David Spergel, Renyue Cen and Xavier Prochaska for useful discussions and comments. He is also grateful to James Bolton for providing covariance matrices from his simulations, and to the anonymous referee for useful criticisms which have improved the paper.

REFERENCES

- Becker, G. D., Bolton, J. S., Haehnelt, M. G., & Sargent, W. L. W. 2011, MNRAS, 410, 1096
- Becker, G. D., Rauch, M., & Sargent, W. L. W. 2007, ApJ, 662, 72
- Bolton, J. S., Haehnelt, M. G., Viel, M., & Springel, V. 2005, MNRAS, 357, 1178
- Bolton, J. S., Viel, M., Kim, T., Haehnelt, M. G., & Carswell, R. F. 2008, MNRAS, 386, 1131
- Cen, R. & Chisari, N. E. 2010, ArXiv e-prints
- Cen, R., Miralda-Escudé, J., Ostriker, J. P., & Rauch, M. 1994, ApJ, 437, L9
- Croft, R. A. C., Weinberg, D. H., Bolte, M., Burles, S., Hernquist, L., Katz, N., Kirkman, D., & Tytler, D. 2002, ApJ, 581, 20
- Croft, R. A. C., Weinberg, D. H., Katz, N., & Hernquist, L. 1998, ApJ, 495, 44
- Dall’Aglia, A., Wisotzki, L., & Worseck, G. 2009, ArXiv e-prints
- Davé, R., Hernquist, L., Katz, N., & Weinberg, D. H. 1999, ApJ, 511, 521
- Faucher-Giguère, C., Lidz, A., Hernquist, L., & Zaldarriaga, M. 2008a, ApJ, 682, L9
- Faucher-Giguère, C., Prochaska, J. X., Lidz, A., Hernquist, L., & Zaldarriaga, M. 2008b, ApJ, 681, 831
- Furlanetto, S. R. & Oh, S. P. 2008, ApJ, 681, 1
- Giallongo, E., Cristiani, S., & Trevese, D. 1992, ApJ, 398, L9
- Gunn, J. E. & Peterson, B. A. 1965, ApJ, 142, 1633
- Hui, L. & Gnedin, N. Y. 1997, MNRAS, 292, 27
- Jenkins, E. B. & Ostriker, J. P. 1991, ApJ, 376, 33

- Kim, T., Bolton, J. S., Viel, M., Haehnelt, M. G., & Carswell, R. F. 2007, *MNRAS*, 382, 1657
- McDonald, P., Miralda-Escudé, J., Rauch, M., Sargent, W. L. W., Barlow, T. A., Cen, R., & Ostriker, J. P. 2000, *ApJ*, 543, 1
- McDonald, P., Seljak, U., Cen, R., Shih, D., Weinberg, D. H., Burles, S., Schneider, D. P., Schlegel, D. J., Bahcall, N. A., Briggs, J. W., Brinkmann, J., Fukugita, M., Ivezić, Ž., Kent, S., & Vanden Berk, D. E. 2005, *ApJ*, 635, 761
- McQuinn, M., Lidz, A., Zaldarriaga, M., Hernquist, L., Hopkins, P. F., Dutta, S., & Faucher-Giguère, C. 2009, *ApJ*, 694, 842
- Meiksin, A. & White, M. 2004, *MNRAS*, 350, 1107
- Miralda-Escudé, J., Cen, R., Ostriker, J. P., & Rauch, M. 1996, *ApJ*, 471, 582
- Miralda-Escudé, J., Haehnelt, M., & Rees, M. J. 2000, *ApJ*, 530, 1
- Sargent, W. L. W., Young, P. J., Boksenberg, A., & Tytler, D. 1980, *ApJS*, 42, 41
- Schaye, J., Theuns, T., Rauch, M., Efstathiou, G., & Sargent, W. L. W. 2000, *MNRAS*, 318, 817
- Scott, J., Bechtold, J., Dobrzycki, A., & Kulkarni, V. P. 2000, *ApJS*, 130, 67
- Theuns, T., Leonard, A., Efstathiou, G., Pearce, F. R., & Thomas, P. A. 1998, *MNRAS*, 301, 478
- Viel, M., Bolton, J. S., & Haehnelt, M. G. 2009, *MNRAS*, 399, L39
- White, M., Pope, A., Carlson, J., Heitmann, K., Habib, S., Fasel, P., Daniel, D., & Lukic, Z. 2010, *ApJ*, 713, 383
- Zaldarriaga, M., Scoccimarro, R., & Hui, L. 2003, *ApJ*, 590, 1